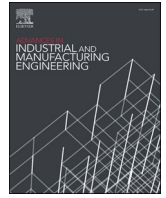# Mathematical model for heat transfer during laser material processing.

MOSTAFA, A. and HOSSAIN, M.

2022

Contents lists available at ScienceDirect

Advances in Industrial and Manufacturing Engineering

journal homepage: www.sciencedirect.com/journal/advances-in-industrial-and-manufacturing-engineering

Mathematical model for heat transfer during laser material processing

Ayman Mostafa [*], Mamdud Hossain

School of Engineering, Robert Gordon University, Garthdee Road, Aberdeen, AB10 7GJ, UK

A B S T R A C T

The article presents development of a new heat transfer model for calculating temperature distribution in porous and non-porous materials during laser cutting. The novelty of this model lies in incorporating melting and vaporization progression of porous media during laser interaction. The modelling has been implemented through a transient finite difference scheme and the results have been validated against experimental data of cutting various materials by laser including rock and metals.

1. Introduction

Waste power due to heat transfer into surrounding during laser material processing is a transient process which is complex to be calculated analytically and accordingly a numerical solution would be required.

Most of the mathematical models developed in the past to simulate heat transfer and temperature distribution during laser material processing were conducted for metals and they are needed to be modified for modelling heat transfer in porous media such as laser cutting of cloths or reservoir.

Sheng and Joshi (1995) developed a 2D finite element model to simulate Heat Affected Zone (HAZ) during laser cutting of stainless steel. The cutting front geometry was calculated analytically and temperature distribution calculated numerically. The results showed a good agreement with laser cutting experiments. Latent heat and phase changes were considered in the analytical model but not in the heat transfer numerical model.

Modest (1996) developed a 3D finite difference model to predict the transient temperature distribution inside a thick solid during laser ablation (solid material decomposition) including continuous wave and pulsed laser modes. The results showed that conduction losses during short-pulsed laser ablation are negligible, resulting in larger removal rates compared to continuous wave's operation. However, Modest assumed that phase changing from solid to vapour occurs in a single step by employing the total amount of energy required to remove material.

Verhoeven et al. (2003) developed a 1D finite element model to simulate laser drilling. Dimensionless enthalpy was considered to incorporate the latent heat of melting and vaporization. However, the

model assumed that radial heat transfer is negligible which is probably suitable for the scale of this model but it usually has a significant impact in most of laser applications.

Otto et al. (2012) developed a 1D finite volume model to simulate a wide range of laser material processing and pointed out that simulation remains a difficult task despite of strong efforts done in the past due to the complexity of laser processes where a variety of different physical phenomena are coupled. However, the model considered latent heat and phase changes in the direction of laser interaction (one-dimensional) but not the radial heat transfer into surrounding.

Fu et al. (2014) developed a 3D finite element model to simulate laser cutting of nitinol alloys using pulsed laser. The predicted kerf geometry and HAZ were verified by experimental data. However, it is not clear if latent heat and phase changing were considered in the heat flux model.

As shown above, the models developed in the past are similar in principle where energy balance equations were numerically solved by finite element, finite difference or finite volume methods. Despite the numerous modelling conducted in the past, the majority of them were focused on metals. There is a lack of literature regarding the modelling of laser material processing in porous media.

Porous media could be any type of rocks including sedimentary rocks with high porosity such as sandstone and limestone or basement rocks with very low porosity such as granite and marble. The alloy powder beds used in Additive Layer Manufacturing (ALM) and Selective Laser Melting (SLM) as well as nonwoven fibers could be treated as porous media with interconnected voids.

Examples of laser powder bed modelling are the simulation model developed by Kundakcioglu et al. (2016) to predict transient

---

temperature fields in additive layer manufacturing (ALM) of a 3D complex structures and the model developed by Pei et al. (2017) to simulate Selective Laser Melting (SLM) of A1Si10Mg powder. However, Powder bed technique relay on melting the bed layers selectivity and focus on optimum hatch spacing and scanning speed required to produce dense and smooth surface after processing which is different application compared to laser cutting.

This paper suggests a novel and robust mathematical model which can be used to model heat transfer during laser material processing in porous media where melting and vaporization progression during laser interaction with the material and fluids in the porous media have been considered and incorporated into the model. However, the effect of porous morphology is not considered in this work.

The model has been validated with Continuous Wave (CW) and pulsed laser cutting for metals and non-metals so it can also be used for modelling non porous media. It can be used for modelling laser cutting and drilling applications. In addition, various heat-source boundary conditions have been considered and suggested for various cutting techniques including cutting-by-melting and cutting-by-vaporization.

The novelty of this model lies in incorporating melting and vaporization progression into the heat balance equation, and accordingly this model could be considered as an ideal approach for modelling materials having wide ranges of melting (or vaporization) progression and materials that produce mushy region during melting such as alloys substances, especially if the interval around melting temperature, where solid and liquid exist simultaneously, is known or can be measured in laboratory.

2. Methodology

There are three sources of heat transfer into surrounding during laser material processing including conduction, convection and radiation. Powell et al. (1994) pointed out that convective and radiative losses are negligible but conductive losses are considerable. Powell's work is also cited by Webb and Jones (2004) in the Handbook of laser technology and applications.

The major source of heat losses during laser material processing is conduction while the contribution of convection and radiation are very small and can be neglected (Prusa et al., 1999).

2.1. Heat transfer equation

Unsteady-state (transient) conduction heat transfer in cylindrical and axial coordinates can be described by the following partial differential equation (Bennett and Myers, 1983):

$$\frac{\partial T}{\partial t} = \alpha \left(\frac{\partial^2 T}{\partial r^2} + \frac{1}{r} \frac{\partial T}{\partial r} + \frac{\partial^2 T}{\partial x^2} \right) \tag{1}$$

Where T is temperature in Kelvin, t is time in second, r is radius in cylindrical coordinates in meter, x is distance in axial coordinates in meter and α is thermal diffusively in m^2/sec and equal $k/\rho\, c_p$ where k is thermal conductivity in $W/m\,K$, ρ is density in kg/m^3 and c_p is specific heat capacity at constant pressure in $J/kg\,K$.

It is assumed that there is no variation on temperature with angular position and accordingly the angular term, $\frac{1}{r^2} \frac{\partial^2 T}{\partial \theta^2}$, is already omitted from the above equation.

2.2. Latent heat and melting fraction

In order to model the effect of melting progression of the porous media on heat transfer into surrounding during laser interaction, a modification is made to the partial differential equation by adding melt fraction and latent heat of melting.

Hossain et al. (2005) described the transient heat transfer and

melting process of nonwoven fibers by adding latent heat of fusion L_f (J/kg) and liquid (melt) fraction γ (dimensionless) into the energy equation where γ is a function of temperature as following:

$$\gamma = \begin{cases} 1 \;\; if\; T > T_m + \Delta T \,(complete\; liquid\; state) \\ 0 \;\; if\; T < T_m - \Delta T \,(complete\; solid\; state) \\ \dfrac{T - T_m + \Delta T}{2\Delta T} \;\; if\; T_m - \Delta T < T < T_m + \Delta T \,(phase\; changing\; 0 < \gamma < 1) \end{cases} \tag{2}$$

Where T is the mean temperature in Kelvin, T_m is melting temperature in Kelvin and ΔT is a small temperature interval around the melting temperature as solid and liquid may exist simultaneously in a volume element if temperature is within a small interval $2\Delta T$ around the melting temperature as shown in Fig. 1.

The modified partial differential equation after adding the latent heat of fusion and melt fraction (has been defined here as γ_m) is shown below:

$$\frac{\partial T}{\partial t} = \alpha \left(\frac{\partial^2 T}{\partial r^2} + \frac{1}{r} \frac{\partial T}{\partial r} + \frac{\partial^2 T}{\partial x^2} \right) - \frac{L_f}{c_{p_r}} \frac{\partial \gamma_m}{\partial t} \tag{3}$$

Where L_f is latent heat of fusion, c_{p_r} is specific heat capacity at constant pressure for the rock and γ_m is melt fraction. For simplicity, same thermal properties has been assumed for both solid and melt states of the rock.

2.3. Porosity and fluid saturation

Porosity and fluid saturation exist in porous media have been incorporated into the partial differential equation by considering effective thermal diffusivity and also modelling the vaporization progression for the liquid exists in porous media using the same concept of melting fraction described above.

The modified partial differential equation after adding porosity and fluid saturation can be written as following:

$$\frac{\partial T}{\partial t} = \alpha_{eff} \left(\frac{\partial^2 T}{\partial r^2} + \frac{1}{r} \frac{\partial T}{\partial r} + \frac{\partial^2 T}{\partial x^2} \right) - (1 - \varphi) \frac{L_f}{c_{pr}} \frac{\partial \gamma_m}{\partial t} - \varphi \frac{L_v}{c_{pl}} \frac{\partial \gamma_v}{\partial t} \tag{4}$$

Where;

α_{eff} is effective thermal diffusivity.

$$\alpha_{eff} = \varphi \left(\alpha_w\, S_w + \alpha_o\, S_o + \alpha_g\, S_g \right) + (1 - \varphi)\, \alpha_{rock} \tag{5}$$

φ is porosity, s is fluid saturation in the void space of the porous media, α is thermal diffusivity and subscripts $w,\; o\; and\; g$ refer to water, oil and gas (or air) respectively, and subscript 'rock' represents the solid space of the porous media. Note that rock is used in the equation to represent the porous media. However, any other type of porous media and fluid types
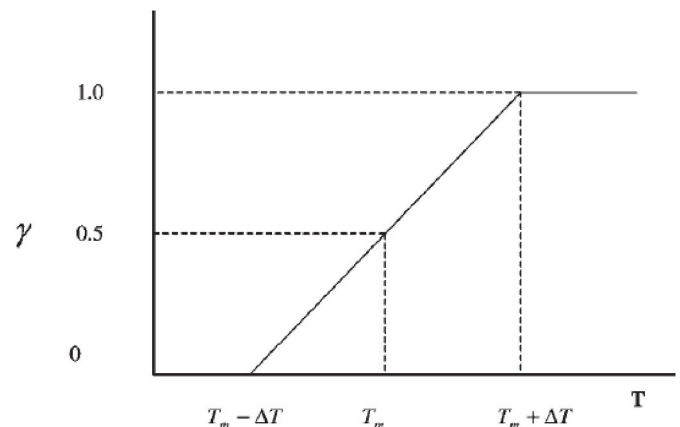
Fig. 1. Variation of melt fraction with temperature (Hossain et al., 2005).

can be considered in the above equation using the same concept.

L_f and c_{p_r} are latent heat of fusion and specific heat capacity of the rock.

L_v and c_{pl} are latent heat of vaporization and specific heat capacity of the liquid exists in porous media.

γ_m is melting fraction of the rock.

γ_v is vaporization fraction of the liquid exists in porous media.

Note that the term $(1-\varphi)\frac{L_f}{c_{p_r}}\frac{\partial\gamma_m}{\partial t}$ represents the melting progression of the rock and the term $\varphi\frac{L_v}{c_{pl}}\frac{\partial\gamma_v}{\partial t}$ represents the vaporization progression of the liquid exists in porous media.

2.4. Finite difference solution

Fig. 2 shows a schematic of laser interaction with one element of porous media in cylindrical coordinates where finite difference method can be used to solve the partial differential equation and model the unsteady-state heat transfer into surrounding in both radial and axial directions during laser interaction with porous media. i and j are the spatial grid system in radial and axial coordinates respectively.

Fig. 3 shows cross-sections of the cylindrical element (heat source) and describes the explicit finite difference solution for radial heat transfer into surrounding in cylindrical coordinates where T at time level $n + 1$ can be calculated using the values of the previous time level n.

T_i^{n+1} can be calculated at all time levels as long as the initial and boundary conditions are known. Note that i represents the spatial radial grid system, Δt is time step and Δr is spatial step in radial coordinates.

Fig. 4 shows cross-sections in the direction of laser cutting and describes the explicit finite difference solution for axial heat transfer into surrounding in the same direction of the laser beam. Note that j represents the spatial grid system in x direction, Δt is time step and Δx is spatial step in axial coordinates.

Finite difference solution is used to solve the partial differential equation and the final equation is shown below:

$$T_{i,j}^{n+1} = \left[\begin{array}{l} \frac{\alpha_{eff}\Delta t}{\Delta r^2}\left(T_{i+1,j}^n + T_{i-1,j}^n\right) \ + \ \frac{\alpha_{eff}\Delta t}{\Delta x^2}\left(T_{i,j+1}^n + T_{i,j-1}^n\right) \\ + \ T_{i,j}^n\left(1 - \frac{2\,\alpha_{eff}\Delta t}{\Delta r^2} - \frac{\alpha_{eff}\Delta t}{r\Delta r} - \frac{2\,\alpha_{eff}\Delta t}{\Delta x^2}\right) \\ - \ (1-\varphi)\frac{L_f}{c_{p_r}}\left(\gamma_{m i,j}^{n+1} - \gamma_{m i,j}^n\right) \ - \ \varphi\,\frac{L_v}{c_{pl}}\left(\gamma_{vi,j}^{n+1} - \gamma_{vi,j}^n\right) \end{array} \right] \Big/ 1 - \frac{\alpha_{eff}\Delta t}{r\Delta r}$$

(6)

This is the appropriate equation to calculate heat transfer into surrounding during laser interaction with porous media including melting and vaporization progression.

3. Results and discussions

The results of the numerical model are discussed in this section

including model geometry, the effect of boundary conditions and model validations.

3.1. Model geometry and numerical stability

The mesh structure was built in cylindrical geometry to model heat transfer in axial and radial coordinates during laser interaction with material as a dynamic heat source moving in the axial coordinate.

Sensitivity analysis was conducted to identify the optimum grid cell sizes in all coordinates including spatial axial step (Δx), spatial radial step (Δr) and time step (Δr). Small grid sizes and steps are required to ensure numerical stability. However, the model is very sensitive to radial step (Δr) as it represents the main space for heat transfer.

It is also dependent on the thermal properties of the material and cutting speed. This means that each material to be modelled at any particular cutting speed would require different grid sizes in order to reach the optimum mesh dimensions just before numerical instability.

Fig. 5 shows an example of the optimum mesh geometry for cutting 10 cm of sandstone (material thickness), 1 mm kerf width at high cutting speed (10 Pe). In this example the material thickness was divided into 100 grid cells in the axial coordinate ($\Delta x = 0.1$ cm), 100 time-levels (n) with $\Delta t = 0.000426776$ s, and radial step $\Delta r = 0.0333$ mm (one-thirtieth of the beam diameter). Note that in case of lower cutting speed (1.0 Pe for example), numerical stability would be achieved at larger Δr (one-eighth of the beam diameter in this example). This large spatial step is required to accommodate the higher heat transfer due to the low speed of the heat source. However, material thermal properties and cutting speed are the main parameters which can affect the optimum mesh sizes and steps required to ensure numerical stability.

3.2. Initial and boundary conditions

Initial condition of the grid system in radial and axial coordinates represents the initial temperature of the system prior to laser interaction with material. Ambient temperature is used when modelling laser material processing at surface (standard condition).

The boundary condition of the heating source generated by laser due to interaction with material is a complex matter and can be predicted and modelled in different ways based on material thickness and cutting method (melting or vaporization). Boundary condition is a dynamic source of heat during laser interaction and can be considered as one of key parameters, and also source of uncertainty, in modelling heat transfer into surrounding (waste energy) during laser material processing.

Two potential boundary conditions have been considered and can be described as following:

1. Line source boundary condition: where source of heat is considered as a moving line, expanding with melting progression. In other words, during melting any element, laser beam will always be in
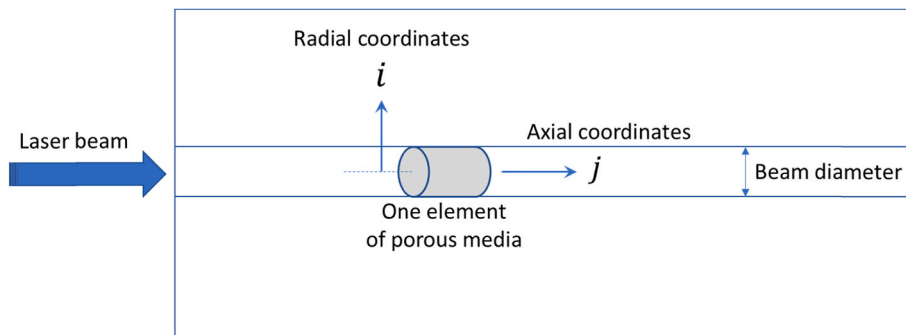

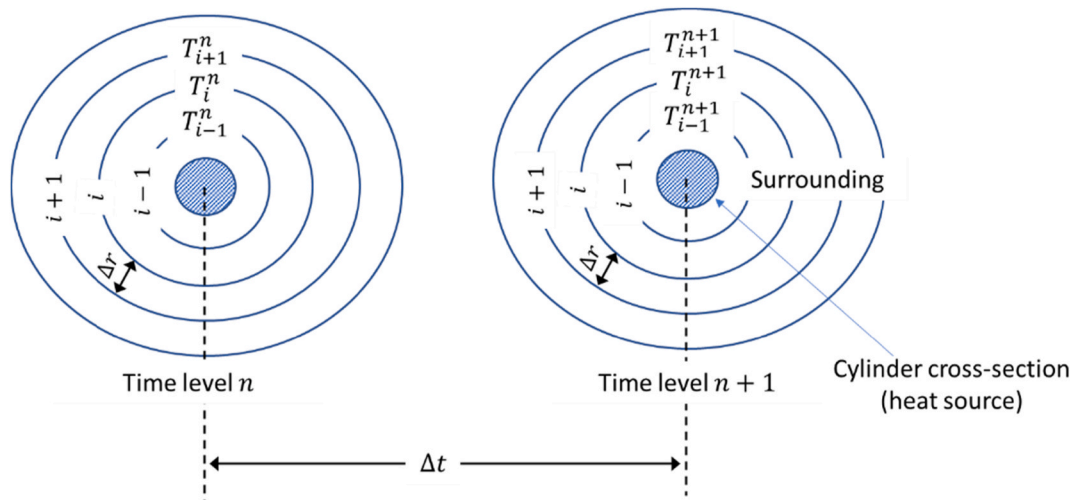**Fig. 2.** Schematic shows heat transfer coordinate systems.

Fig. 3. Radial heat transfer into surrounding (cross-section perpendicular to laser beam).
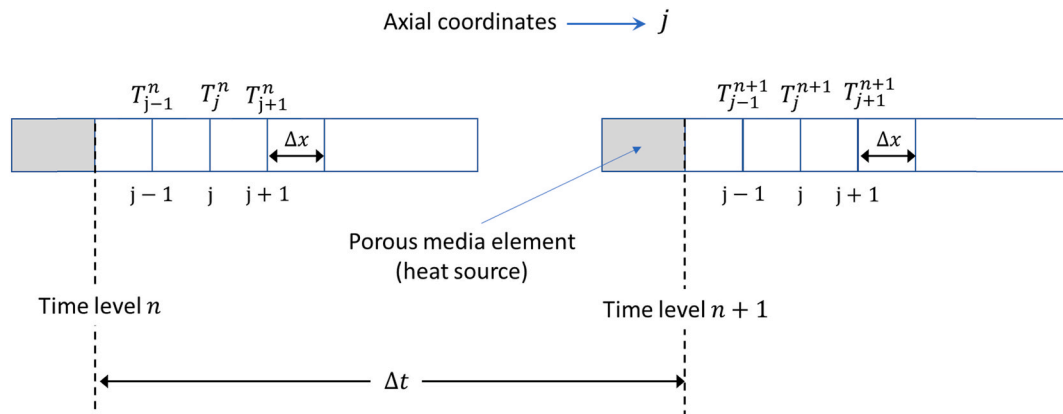

Fig. 4. Axial heat transfer into surrounding (cross-section in the direction of laser cutting).
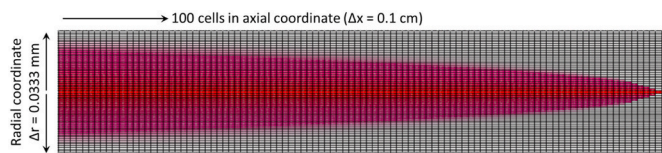

Fig. 5. Model geometry and mesh dimensions (example for cutting 10 cm of sandstone at high cutting speed).

contact with the internal wall of the hole (kerf circumference) for the elements which already melted and cleaned, so laser beam will be considered as a moving line (heating source) during melting progression.

2. Point source boundary condition: where source of heat is considered as only the point of interaction with material at laser beam tip while laser beam is not in contact with the hole already melted, so heating source is like a moving point during melting progression.

3.3. The effect of boundary conditions

Boundary condition has a significant effect in heat transfer into surroundings and waste power during laser cutting accordingly. Fig. 6 shows a comparison of temperature contour between cutting 50 mm thickness of stainless steel at 80 mm/min cutting speed. Significantly higher heat transfer into surrounding is observed for line-source boundary condition compared to point-source because laser beam is always in contact with kerf wall all the time during laser cutting process. This can cause a significant increase in waste power compared to point-source.

3.4. Model's validation

The model has been validated against experimental data for cutting metals (mild steel, stainless steel and aluminium) and non-metals (porous media). Validation has been conducted with various experimental tests as described below.

The numerical model represents the waste power due to heat transfer into surrounding. However, in order to validate the model with the experiments used total laser power rather than waste power, useful power was calculated analytically and added to the modelled waste power. Note that useful power is the power required to remove particular volume of material by melting or vaporization and total power is the sum of both useful and waste powers.

The laser processing parameters used in the experiments such as cutting speed, kerf width and material thickness have been used to set up the boundary conditions in the numerical model, which represent the dynamic heat source and required to calculate heat transfer into surrounding (waste power). Laser parameters also used to analytically calculate the useful power, then validation was conducted by comparing the laser power used in the experiments to the calculated laser power (model's outputs).
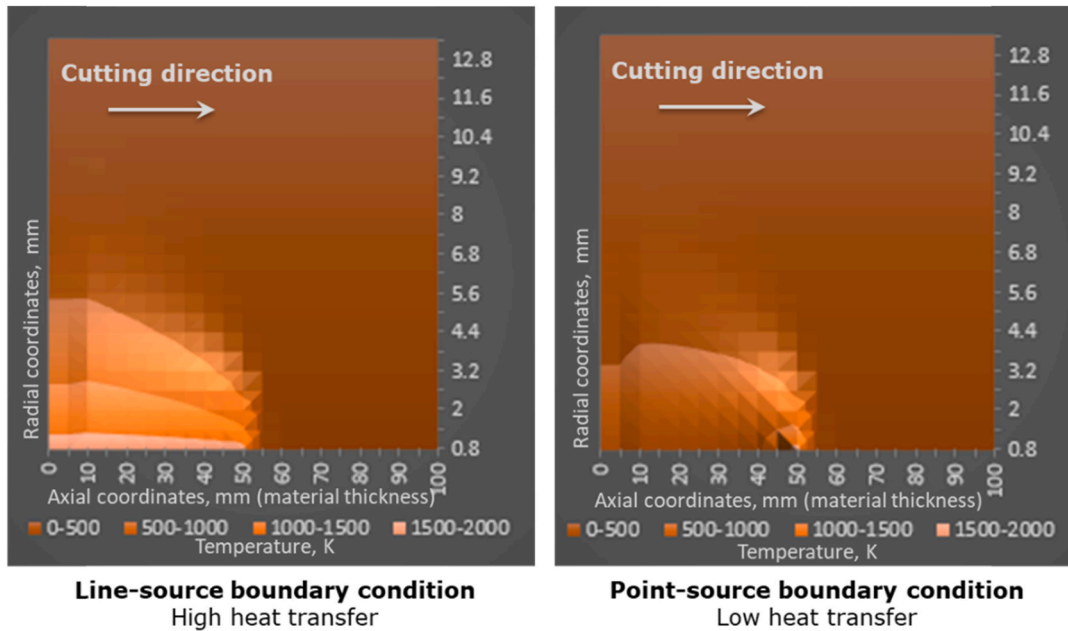
Fig. 6. Comparison between line-source and point-source boundary conditions.

3.4.1. Validation-1 (pulsed Nd:YAG laser drilling in limestone rock)

The experimental test conducted by Erfan et al. (2010) for drilling limestone rock using Nd:YAG pulsed laser is used in model validation-1. The test was conducted by exposing limestone samples to laser radiation and nitrogen was used as gas purging to clean the molten material out of the hole. The radiation time, drilling depth and speed were measured, then specific energy was calculated accordingly.

Specific Energy (SE), as defined by Erfan et al., is the energy required to remove a given volume of rock (SE = energy input/volume). Erfan calculated specific energy from the laser energy used in the experiment and the volume of rock removed during laser drilling.

The same parameters and drilling geometry achieved in the experiment (drilling thickness, speed and irradiation time) have been used in the model to replicate the same experiment condition and calculate the laser power. Energy is calculated based on power and irradiation time (Energy = power x irradiation time), then specific energy is calculated based on energy and drilling geometry (the volume of rock removed).

Eventually, in order to validate the model, the specific energy calculated using the model outputs is compared with the specific energy calculated from the experiment parameters and reported by Erfan et al. Note that specific energy is used for comparison rather than laser power because only specific energy was reported by Erfan et al. (not the actual laser power used in the experiment).

Table 1 shows the experimental data and comparison between the specific energy calculated in the experiment and reported by Erfan et al. and the calculated specific energy from the model.

Laser beam diameter was not reported and an average of 1 mm is

assumed in the model. However the comparisons are based on specific energy (per unit volume) rather than the actual power used and accordingly this assumption might be associated with a marginal error. The reported rock porosity is within 5–15%. However, an average porosity of 10% is assumed in the model.

Fig. 7 shows the results of validation-1 including comparison between experimental data and models results for water saturated limestone rock. Similar results are observed for oil saturated and dry rock tests.

The results showed that line-source numerical model matches the experimental data with 5–15% deviation, while point-source numerical model is lower than experimental data by 28–42%. Point-source boundary condition model underestimates the laser power requirements in this experiments. The results indicated that line-source could be the most suitable boundary condition for modelling pulsed laser drilling and cutting by melting techniques.

3.4.2. Validation-2 (CO2 laser cutting by vaporization in limestone rock)

The experimental test conducted by Carstens and Brown (1971) is used in validation-2. This test was conducted by cutting limestone rock using CO_2 laser power level of 3–4 kW to study the feasibility of using

Table 1
Model validation-1, experimental data and specific energy (SE) comparison.

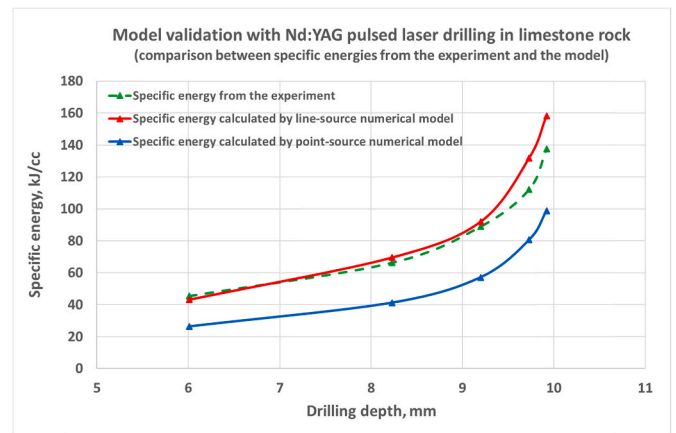| Material	Thickness (drilling depth), mm	Drilling speed (ROP), mm/s	SE from the exp., KJ/cc	SE calculated from the model, KJ/cc	
				Line-source model	Point-source model
Limestone rock (water saturated)	6.01	1.20	45.38	43.22	26.40
	8.23	0.82	66.28	69.62	41.32
	9.20	0.61	88.94	91.98	57.20
	9.73	0.49	112.12	131.69	80.59
	9.92	0.40	137.47	158.17	98.83

Fig. 7. Model validation-1 results (Nd:YAG pulsed laser drilling in limestone rock).

laser to assist mechanical rock tunneling. Table 2 shows the experimental data and comparison between the actual total power used in the experiment and the calculated total power.

Clean cuts with almost no melt zone were created in this test without gas purging, which means rock vaporization temperature was reached and accordingly cutting by vaporization is considered in laser power modelling of this test.

Dry sample with an average porosity of 10% is assumed, and also an average kerf width of 1 mm is assumed (average from the rock sample's cross-section provided after laser cutting). Fig. 8 shows the results of model validation-2 including comparison between experimental data and models results.

The results showed that numerical point-source model is very close to the laser power level used in the test (good match), while numerical line-source model is higher than the experimental data. Point-source boundary condition is more relevant and better representing cutting by vaporization method. Point-source boundary condition yields lower heat transfer into surrounding because laser beam will not be in contact with kerf wall once material evaporated.

3.4.3. Validation-3 (cutting thick stainless-steel using fiber laser)

This test was conducted by Shin et al. (2019) for the purposes of dismantling nuclear facilities. Cutting by melting of 50 and 60 mm thick stainless-steel plates was conducted in air and underwater using 6 kW fiber laser and compressed air as gas purging. Table 3 shows the experimental data and comparison between the actual total power used in the experiment and the calculated total power.

Fig. 9 shows model validation-3 results including comparison between experimental data and models results for cutting 50–60 mm stainless-steel plates.

The results showed that experimental data is perfectly matched with line-source numerical model with only 2% deviation (except one point with 13% deviation), while point-source numerical model is lower than experimental data by 35–44%.
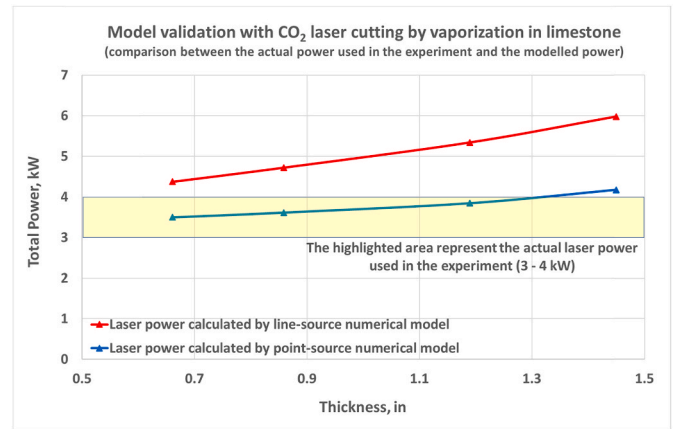
3.4.4. Validation-4 (cutting mild and stainless steel with CO2 laser and oxygen gas assist)

This experimental work was conducted by Powell et al. (1994) to measure the waste energy during laser cutting of mild and stainless steel. 50 mm diameter circle discs with various thicknesses were cut at maximum possible speed using 800 W CO2 laser power and oxygen gas assist.

The discs were placed in an insulated water bath immediately after cutting in order to measure the absorbed heat. Table 4 shows the experimental data and comparison between the actual waste power

Fig. 8. Model validation-2 results (CO2 laser cutting by vaporization in limestone rock).

measured in the experiment and the calculated waste power. Note that the experimental waste power data has been calculated based on the measured absorbed heat.

Fig. 10 shows model validation-4 results including comparison between experimental data and models results for cutting mild steel using CO2 laser and oxygen gas assist.

The results showed that the experimental data of cutting mild steel is located between line-source and point-source models. However, low thickness points (higher cutting speed) showed better matching with line-source model, while high thickness points (lower cutting speed) showed better matching with point-source model. Note that the experimental data for stainless-steel couldn't be matched with the models. Experimental waste power for stainless-steel is approximately three times higher than the models results.

There are many uncertainties in this experiment which could affect the accuracy of the validation results and mislead the interpretation, including the following:

1. The heat losses were measured in the cut disc then it was doubled assuming equal heat losses was occurred (transferred) into the other side of the material, which is not necessarily correct. This assumptions (approximation) might significantly affect the validation results.
2. Thermal properties for the materials used in the experiment are not available. There is a wide range of stainless-steel grades with different thermal properties and this could be the reason of the mismatching observed with stainless-steel experimental data.
3. The experiment showed that stainless steel heat losses was significantly higher than mild steel, while the thermal conductivity of stainless steel is generally lower than mild steel.
4. The experimental waste power exceeded the total laser power used (800 W). This is due to the extra heat generated by oxidation as oxygen gas assist was used. This wouldn't affect the accuracy of the validation because the comparison was made for waste power rather than total laser power.

3.4.5. Validation-5 (cutting stainless steel and aluminium with CO2 laser and nitrogen gas)

The experimental data presented by Webb and Jones (2004) is used in model validation-5. This data represents average (approximate) laser

Table 2
Model validation-2, experimental data and power comparison.

Material	Thickness, inch	Cutting speed, inch/min	Total power, used in the exp., kW	Total power, calculated, kW	
				Line-source model	Point-source model
Limestone rock	0.661	13.2	3–4	4.37	3.50
	0.859	10.4	3–4	4.72	3.61
	1.190	7.9	3–4	5.34	3.84
	1.450	7.0	3–4	5.98	4.17

Table 3

Model validation-3, experimental data and power comparison.

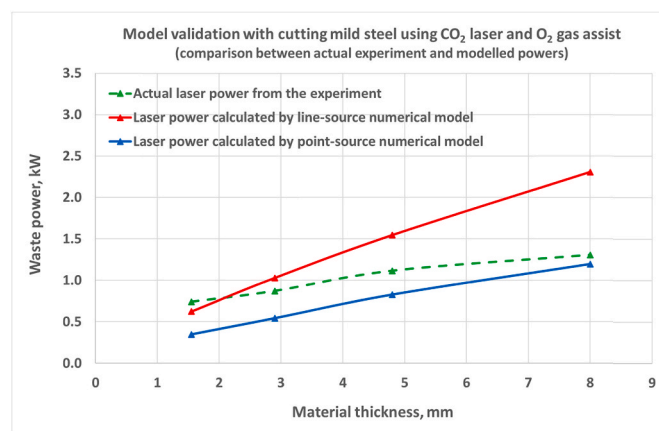| Material	Thickness, mm	Cutting speed, mm/min	Kerf width, mm	Total power used in the exp., kW	Total power, calculated, kW	
					Line-source model	Point-source model
Stainless-steel (in air)	50	140	1.1	6	6.2	3.9
	60	90	1.1	6	6.8	4.0
Stainless-steel (underwater)	50	100	1.4	6	5.8	3.8
	60	40	1.4	6	6.1	3.4
	50	80	1.6	6	5.9	3.6
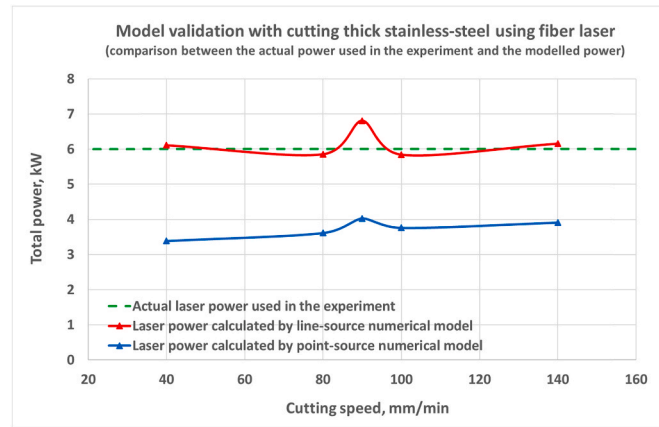
Fig. 9. Model validation-3 results (cutting thick stainless-steel in air and underwater using fiber laser).

Table 4

Model validation-4, experimental data and power comparison.

Material	Thickness, mm	Cutting speed, m/min	Kerf width, mm	Waste power, in the exp., kW	Waste power, calculated, kW	
					Line-source model	Point-source model
Mild-steel	1.55	6.40	0.30	0.74	0.62	0.35
	2.90	3.15	0.30	0.87	1.03	0.54
	4.80	1.80	0.35	1.12	1.55	0.83
	8.00	0.80	0.40	1.31	2.31	1.20
Stainless-steel	1.20	7.70	0.25	0.51	0.24	0.13
	1.90	4.08	0.30	0.93	0.31	0.18
	3.25	2.40	0.35	1.48	0.51	0.27
	5.00	1.53	0.35	2.12	0.73	0.38

Fig. 10. Model validation-4 results (cutting mild steel with CO2 laser and oxygen gas assist).

Table 5
Model validation-5, experimental data and power comparison.

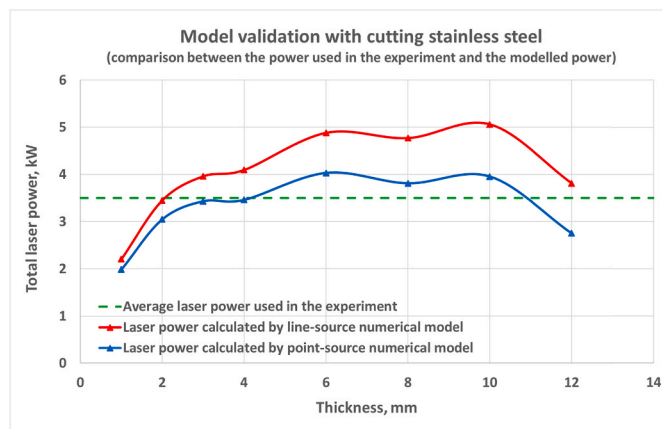| Material	Thickness, mm	Approx. max. cutting speed, m/min	Nozzle diam., mm	Total power, used in the exp., kW	Total power calculated, kW	
					Line-source model	Point-source model
Stainless-steel	1	10	1.5	3.50	2.21	1.99
	2	6.6	1.7	3.50	3.45	3.05
	3	4.1	2.0	3.50	3.96	3.43
	4	3	2.0	3.50	4.09	3.46
	6	1.8	2.5	3.50	4.88	4.03
	8	1.2	2.5	3.50	4.77	3.81
	10	0.8	3.0	3.50	5.06	3.95
	12	0.4	3.0	3.50	3.81	2.75
Aluminium	2	7	1.7	3.50	2.55	2.03
	3	4	2.0	3.50	3.12	2.37
	4	3	2.0	3.50	3.70	2.62
	5	2	2.0	3.50	3.93	2.68
	6	1	2.5	3.50	3.72	2.84

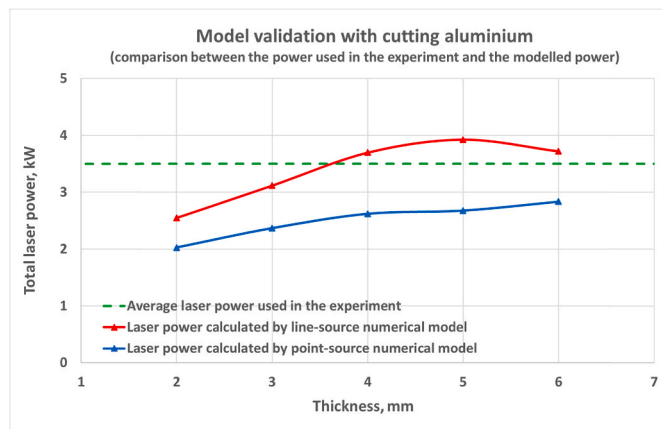**Fig. 11.** Model validation-5 results (cutting stainless steel).

Fig. 12. Model validation-5 results (cutting aluminium).

processing parameters required to cut various material thickness of stainless-steel and aluminium using CO2 laser and nitrogen gas purging. Table 5 shows the experimental data and comparison between the actual total power used in the experiment and the calculated total power.

Fig. 11 and Fig. 12 show the results of model validation-5 including comparison between experimental data and model results for stainless steel and aluminium respectively.

Numerical point-source model showed better matching with stainless-steel experimental data, while line-source model showed better matching with aluminium data. (note the uncertainty in stainless steel thermal properties).

The following is a summary of the uncertainties and assumptions made in this validation which may affect the accuracy of the results:

1. The data presented by Webb and Jones represents average (approximate) laser processing parameters and should be used as guideline only. Perfect matching is not expected accordingly.
2. The reported nozzle diameters are assumed to be similar to kerf widths, which it is not necessarily correct.
3. Thermal properties of the material used in the experiments are not available and this can affect the accuracy of the validation results especially for stainless-steel where wide range of grades are available.

Although perfect matching is not expected in validation-5, the results showed a good overall matching with line-source model considering the uncertainty in the thermal properties of the stainless steel grade used in this experiments.

4. Conclusions

A mathematical model for heat transfer during laser cutting in porous media has been developed and presented in this paper. Partial differential equation for transient heat transfer in cylindrical and axial coordinates has been used as a base heat balance equation to simulate temperature distribution and waste energy during laser cutting. The equation solved using finite difference scheme.

The partial differential equation has been modified by incorporating porosity, fluid saturations, latent heat of fusion and vaporizations, melting and vaporization fractions in order to simulate the actual physics of phase changing progression in porous media during laser material processing.

The novelty of this model lies in incorporating melting and vaporization progression into the heat balance equation, and accordingly it is suitable for modelling materials having wide ranges of melting (or vaporization) temperatures and materials that produce mushy region during melting progression such as alloys substances.

Boundary condition is one of the key parameters, and also source of uncertainty, in modelling heat transfer which represents the dynamic source of heat during laser interaction. Line-source and point-source boundary conditions have been suggested and discussed.

The model has been validated by experimental data and showed good corroboration for metal and non-metal (porous media). Line-source and point source boundary conditions showed good matching with laser cutting-by-melting and cutting-by-vaporization respectively. Model's validations also showed that the model can be used for laser drilling as well as laser cutting applications.

This model can be used for pulsed and Continues Wave (CW) lasers and for various laser applications including cutting and drilling (by-

melting and by-vaporization). The model can also be used for any other applications to calculate heat losses from any dynamic heat source.

Declaration of competing interest

The authors declare that they have no known competing financial interests or personal relationships that could have appeared to influence the work reported in this paper.

References

Bennett, C.O., Myers, J.E., 1983. Momentum, Heat and Mass Transfer, third ed. McGraw-Hill, Chemical engineering series.

Carstens, J.P., Brown, C.O., 1971. Rock Cutting by Laser. Fall Meeting of the Society of Petroleum Engineers of AIME, p. 11.

Erfan, M.R., et al., 2010. Drilling of Middle-Eastern Reservoir Carbonate Rocks by High Power ND:YAG Laser. IADC/SPE Asia Pacific Drilling Technology Conference and Exhibition, p. 9.

Fu, C.H., Guo, Y.B., Sealy, M.P., 2014. A predictive model and validation of laser cutting of nitinol with a novel moving volumetric pulsed heat flux. J. Mater. Process. Technol. 214 (12), 2926–2934.

Hossain, M., Acar, M., Malalasekera, W., 2005. A mathematical model for airflow and heat transfer through fibrous webs. Proc. IME E J. Process Mech. Eng. 219 (4), 357–366.

Kundakcioglu, E., Lazoglu, I., Rawal, S., 2016. Transient thermal modeling of laser-based additive manufacturing for 3D freeform structures. Int. J. Adv. Manuf. Technol. 85 (1–4), 493–501.

Modest, M.F., 1996. Three-dimensional, transient model for laser machining of ablating/decomposing materials. Int. J. Heat Mass Tran. 39 (2), 221–234.

Otto, A., Koch, H., Vazquez, R.G., 2012. Multiphysical simulation of laser material processing. Phys. Procedia 39, 843–852.

Pei, W., et al., 2017. Numerical simulation and parametric analysis of selective laser melting process of AlSi10Mg powder. Appl. Phys. Mater. Sci. Process 123 (8).

Powell, J., et al., 1994. Energy redistribution in laser cutting. Weld. Res. Abroad 40 (2), 31–37.

Prusa, J.M., Venkitachalam, G., Molian, P.A., 1999. Estimation of heat conduction losses in laser cutting. Int. J. Mach. Tool Manufact. 39 (3), 431–458.

Sheng, P.S., Joshi, V.S., 1995. Analysis of heat-affected zone formation for laser cutting of stainless steel. J. Mater. Process. Technol. 53 (3), 879–892.

Shin, J.S., et al., 2019. Underwater cutting of 50 and 60 mm thick stainless steel plates using a 6-kW fiber laser for dismantling nuclear facilities. Opt Laser. Technol. 115, 1–8.

Verhoeven, J.C.J., et al., 2003. Modelling laser induced melting. Math. Comput. Model. 37 (3), 419–437.

Webb, C., Jones, J., 2004. Handbook of Laser Technology and Applications.